Interaction Between the Prefrontal and Visual Cortices Supports Subjective Fear

Vincent Taschereau-Dumouchel [1-2,*], Marjorie Côté [1-2], Shawn Manuel [1-2], Darius Valevicius [1-2], Cody A. Cushing [3], Aurelio Cortese [4], Mitsuo Kawato [5-6] & Hakwan Lau [7,*]

Affiliations:

1 - Department of Psychiatry and Addictology, Université de Montréal, Montreal, Quebec, Canada
2 - Centre de Recherche de l'Institut Universitaire en Santé Mentale de Montréal, Montreal, Quebec, Canada
3 - Department of Psychology, UCLA, Los Angeles, 90095, USA.
4 - ATR Computational Neuroscience Laboratories, Kyoto, Japan
5 - ATR Brain Information Communication Research Laboratory, Kyoto, Japan
6 - XNef, Inc., Kyoto, Japan
7 - RIKEN Center for Brain Science, Wako, Saitama, Japan.

*** Correspondence should be addressed to:** Vincent Taschereau-Dumouchel (vincent.taschereau-dumouchel@umontreal.ca) and Hakwan Lau (hakwan.lau@riken.jp)

Abstract

It has been reported that threatening and non-threatening visual stimuli can be distinguished based on the multi-voxel patterns of hemodynamic activity in the human ventral visual stream. Do these findings mean that there may be evolutionarily hardwired mechanisms within early perception, for the fast and automatic detection of threat, and maybe even for the generation of the subjective experience of fear? In this human neuroimaging study, we provide evidence that the ventral visual stream may represent affectively neutral visual features that are statistically associated with fear ratings of participants, without representing the subjective experience of fear itself. More specifically, we show that patterns of hemodynamic activity predictive of a specific "fear profile" (i.e., fear ratings reported by a given participant) can be observed in the ventral visual stream whether a participant reports being afraid of the stimuli or not. Further, we found that the multivariate information transmission between ventral visual areas and prefrontal regions distinguished participants who reported being subjectively afraid of the stimuli from those who did not. Together, these findings support the view that the subjective experience of fear may depend on the relevant visual information triggering implicit metacognitive mechanisms in the prefrontal cortex.

Keywords (3-6): fear, prefrontal cortex, subjective experience, amygdala, artificial neural networks

Introduction

Recently, using multivoxel pattern analysis of magnetic resonance imaging (fMRI) data, it was found that one can decode or classify from the patterns of activity in the human visual cortex between threatening and non-threatening visual stimuli seen by the subjects [1,2]. This has led to the intriguing claim that there may be emotional schemas embedded within the human ventral visual system [2].

Taken further, perhaps one provocative interpretation could be that representations of fear itself could be found within the ventral visual stream, reflecting evolutionarily hard-wired mechanisms for the purpose of automatic detection of threat [3,4]. However, an alternative interpretation could also be that, threatening stimuli (i.e., stimuli that some individuals interpret as threatening and likely to generate fear [4–7]), may, statistically, share certain visual features. For instance, some commonly feared animals and insects are likely to share certain shapes and surface texture, such as scales or shells. Accordingly, what the early visual processes represent may not be a prioritized processing of fear-associated visual features or even the representation of subjective fear *per se*, but rather, only objective visual properties that generally or statistically predict fear.

To arbitrate between these two different interpretations, we can find stimuli that are only reported to be subjectively fearful to some human participants, but not others, such as commonly feared animals. That way, we can experimentally dissociate between objective visual stimuli and subjective fear as indicated by self-report by individual subjects. Importantly, using such an approach, we can test if the "fear profile" (i.e., subjective fear ratings of different animal categories reported by a specific participant) of participants reporting subjective fear ("Fear"

group) can also be decoded based on fMRI patterns of activity in participants reporting no subjective fear ("No fear" group). If such decoding turns out to be equally accurate in both groups, this may support the hypothesis that the ventral visual stream only represents neutral visual features typically associated with fear, but not subjective experience of fear *per se*.

To anticipate, this is exactly what we found in this study: decoding fear profiles from fMRI patterns of activity in the ventral visual stream was equally sensitive for participants who reported to be subjectively afraid of the concerned stimuli or not. Further, similar results can be obtained from two different artificial neural networks that were not trained to be sensitive to fear *per se*; the fear profiles of participants in the "Fear" group can also be predicted by these models. Thus, these findings may merely represent objective visual features, which are independently and statistically associated with common fears.

Moreover, we found that the interaction, i.e. information transmission [8], between multiple prefrontal regions and the ventral visual areas, especially the fusiform gyrus and inferotemporal areas, tracked subjective fear as reflected by the different self-reports across individuals. We hypothesize that this mechanism may ultimately reflect the neurobiological basis of subjective fear.

Methods

Participants. Thirty participants (fourteen females, mean age 23.3 ± 4.35 years) were recruited to take part in an fMRI experiment at the *ATR (Advanced Telecommunications Research) - Computational Neuroscience Laboratories* in Japan. Participants were recruited if they presented self-reported "high" or "very high" fear of at least 2 animals in our database using a 7-point Likert scale. Amongst this group, 3 participants were diagnosed with a specific animal phobias

using the Structured Clinical Interview for DSM-IV. Thirty additional participants were also selected from a larger cohort (N = 53) of participants that underwent the same fMRI experiment (see *Study design*). These participants were selected to act as a control group for the purpose of the current study and were included if they presented no "high" or "very high" fear of any animals included in the dataset (3 females, mean age 23.1 ± 2.87 years). For both groups, inclusion criteria were: (a) aged between 18 and 45; (b) no psychotropic medications; (c) no contraindication to magnetic resonance imaging. The inclusion criteria were specified on the recruitment advertisements and verified through screening forms and an additional assessment on the first day of the study. The study was approved by the ATR Research Ethics Board and the participants provided informed written consent.

MRI parameters. Participants had their brain hemodynamic signals measured and recorded in two 3T MRI scanners (Prisma Siemens and Verio Siemens) with a 32-channels head coil at the ATR Brain Activation Imaging Center. During the experiments, we obtained 33 contiguous slices (TR = 2000 ms, TE =30 ms, voxel size = 3 × 3 × 3.5 mm 3, field-of-view = 192 x 192 mm, matrix size = 64 x 64, slice thickness = 3.5 mm, 0 mm slice gap, flip angle = 80 deg) oriented parallel to the AC-PC plane, which covered the entire brain. We also obtained T1-weighted MR images (MP- RAGE; 256 slices, TR = 2250 ms, TE = 3.06 ms, 5 voxel size = 1 × 1 × 1 mm 3, field-of-view= 256 x 256 mm, matrix size = 256 x 256, slice thickness = 1 mm, 0 mm slice gap, TI = 900 ms, flip angle = 9 deg.).

Stimuli presentation in the fMRI scanner. Visual stimuli were projected on a translucent screen using an LCD projector (DLAG150CL,Victor). The projected image spanned 20 × 15 deg in visual angle (800 × 600 resolution) and had a refresh rate of 60 Hz. The experiment presentation

was conducted using the PsychoPy2 software (v1.83) [9] and images covered 13.33 degrees of visual angles during the procedure.

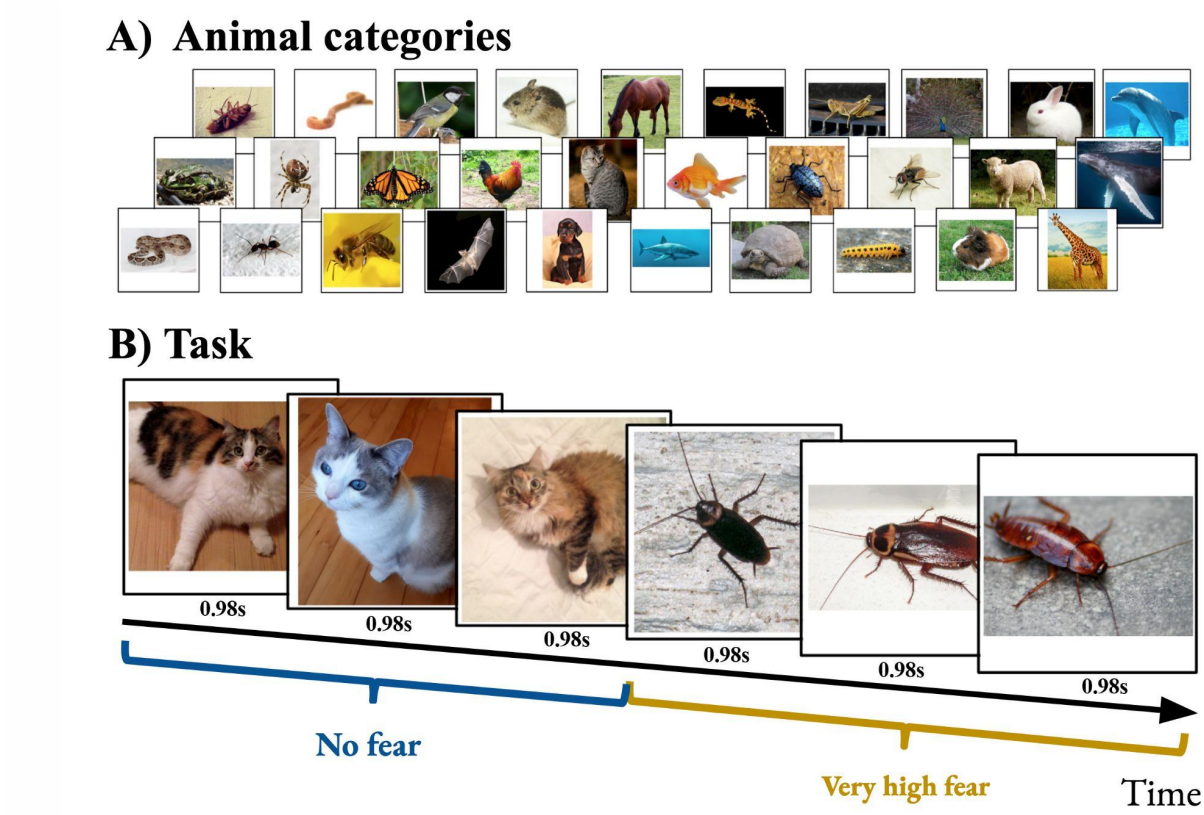

Figure 1. (A) Animal categories included in the fMRI experiment (see text for a complete list). (B) Participants were presented with a series of 3600 images of animals and human-made objects, each lasting 0.98 s. They were asked to pay attention to the image category and report any category change (e.g. from 'cat' to 'cockroach' as shown in the figure) with a button press.

Image presentation. Participants were presented with 3,600 pictures of animals and objects grouped in mini-blocks of 2, 3, 4 or 6 images of the same basic category. Trials were organized into six runs of 600 trials interleaved with short breaks. To make sure that participants paid attention to image categories, they were asked to report any change in category (e.g. from one kind of animal to another) by pressing a button using their right hand. The sequence of image presentation was pseudo-randomized and fixed across participants. In order to allow high-pass

filtering of the fMRI data, chunks within each category were organized so that their period was always shorter than 120 seconds.

We included 90 images of each of the animal and object categories. The 30 animal categories included reptiles (snake and gecko), amphibians (frog and turtle), insects (cockroach, beetle, ant, spider, grasshopper, caterpillar, bee, butterfly, and fly), birds (robin, peacock, and chicken), annelids (earthworm), mammals (mouse, guinea pig, bat, dog, sheep, cat, rabbit, horse, and giraffe) and aquatic animals (shark, whale, common fish, and dolphin). The human-made objects included: airplane, car, bicycle, scissor, hammer, key, guitar, cellphone, umbrella, and chair. The data from the human-made objects were not analyzed in the current project as we focused on animal fear. The 3600 images were collected from various sources on the Internet, including: the Creative Common initiative (https://creativecommons.org), Pixabay (images marked for commercial use and modifications; http://pixabay.com), Flickr (images allowing commercial use and modifications; http://www.flickr.com), and Shutterstock (http://shutterstock.com). The images were selected if they presented a full frontal view of the object or animal and if no other objects were clearly identifiable in the background. Images were cropped so that they would frame the object. The final images were 533 X 533 pixels and covered 13.33 degrees of visual angles during the procedure. The average contrast and luminance of images were not different between categories (see supplementary material of [10]).

Data Analysis

Data pre-processing. MRI results included in this manuscript come from preprocessing performed using fMRIPrep 1.5.9 ([11]; RRID:SCR_016216), which is based on Nipype 1.4.2 ([12,13]; RRID:SCR_002502).

Anatomical data preprocessing. The T1-weighted (T1w) image was corrected for intensity non-uniformity (INU) with N4BiasFieldCorrection [14], distributed with ANTs 2.2.0 ([15], RRID:SCR_004757), and used as T1w-reference throughout the workflow. The T1w-reference was then skull-stripped with a Nipype implementation of the antsBrainExtraction.sh workflow (from ANTs), using OASIS30ANTs as target template. Brain tissue segmentation of cerebrospinal fluid (CSF), white-matter (WM) and gray-matter (GM) was performed on the brain-extracted T1w using fast (FSL 5.0.9, RRID:SCR_002823, [16]). Brain surfaces were reconstructed using recon-all (FreeSurfer 6.0.1, RRID:SCR_001847, [17]), and the brain mask estimated previously was refined with a custom variation of the method to reconcile ANTs-derived and FreeSurfer-derived segmentations of the cortical gray-matter of Mindboggle (RRID:SCR_002438, [18]). Volume-based spatial normalization to one standard space (MNI152NLin2009cAsym) was performed through nonlinear registration with antsRegistration (ANTs 2.2.0), using brain-extracted versions of both T1w reference and the T1w template. The following template was selected for spatial normalization: ICBM 152 Nonlinear Asymmetrical template version 2009c [[19], RRID:SCR_008796; TemplateFlow ID: MNI152NLin2009cAsym].

Functional data preprocessing. For each of the 6 BOLD runs per subject, the following preprocessing was performed: First, a reference volume and its skull-stripped version were generated using a custom methodology of fMRIPrep. Susceptibility distortion correction (SDC) was omitted. The BOLD reference was then co-registered to the T1w reference using bbregister (FreeSurfer) which implements boundary-based registration [20]. Co-registration was configured with six degrees of freedom. Head-motion parameters with respect to the BOLD reference (transformation matrices, and six corresponding rotation and translation parameters) are

estimated before any spatiotemporal filtering using mcflirt (FSL 5.0.9, [21]). BOLD runs were slice-time corrected using 3dTshift from AFNI 20160207 ([22], RRID:SCR_005927). The BOLD time-series were resampled to surfaces on the following spaces: fsaverage5. The BOLD time-series (including slice-timing correction when applied) were resampled onto their original, native space by applying the transforms to correct for head-motion. These resampled BOLD time-series will be referred to as preprocessed BOLD in original space, or just preprocessed BOLD. The BOLD time-series were resampled into standard space, generating a preprocessed BOLD run in ['MNI152NLin2009cAsym'] space. A reference volume and its skull-stripped version were generated using a custom methodology of fMRIPrep. Gridded (volumetric) resamplings were performed using antsApplyTransforms (ANTs), configured with Lanczos interpolation to minimize the smoothing effects of other kernels [23]. Many internal operations of fMRIPrep use Nilearn 0.6.1 (Abraham et al. 2014, RRID:SCR_001362), mostly within the functional processing workflow. For more details of the pipeline, see the section corresponding to workflows in fMRIPrep's documentation.

NiLearn [24] was used to detrend, remove motion confounds (24 parameters: 3 rotations, 3 translations, their time derivatives, power 2, and derivative power 2) and standardize data. Single-trial estimates were then obtained using the least-square separate approach [25,26] implemented using functions from pyMVPA [27,28]. This method allows to iteratively fit a general linear model to estimate the brain response to each image. Each general linear model includes one parameter modeling the current trial and two parameters modeling all other trials in the design.

Decoding fear profiles in the ventral visual stream. We used single-trial estimates of brain activity to predict the reported level of fear within-participants (0 = "No fear" to 5 = "Very high

fear"). However, since the distribution of fear ratings tended to be skewed (i.e. many participants reported a disproportionate number of categories eliciting "No Fear"), we randomly under-sampled the "No Fear" level to match the mean number of trials in other fear levels. After under-sampling, the mean number of trials was 1857.2 ± 612 trials.

Decoding was achieved using a 6-fold cross-validation, as a function of experimental blocks, using LASSO regression as implemented in Scikit-Learn [29]. We used the Fisher-transformed correlation coefficient between the predicted and real values as a metric of performance. Decoding was conducted within 4 regions of the ventral visual stream: occipital cortex, fusiform gyrus, inferior temporal gyrus and middle temporal gyrus. The regions of interest were determined as a function of the Brainnetome Atlas annotation [30]. Masks of the 4 ventral visual regions are illustrated in Fig. 3.

Decoding performances were computed in the "Fear" group and compared to the decoding of the same fear profile in the "No fear" group. This was achieved in order to determine if the same decoding performance could be obtained in participants reporting no subjective fear of the presented animals. In order to do so, we used the fear ratings of each participant in the "Fear" group and predicted these fear ratings from the brain activity of each of the 30 participants in the "No fear" group (i.e., 30 X 30 decoders). Paired-sample t-tests were used to compare the mean predictions of a given fear profile in the "No Fear" group to the prediction of the corresponding participant in the "Fear" group. The Bonferroni correction was used to control for multiple comparisons (4 ROIs) and the Bayesian paired-sample t-tests were used to determine the likelihood of rejecting the null hypothesis. One sample t-tests were also used to determine above chance performance and corrected for multiple comparisons using the Bonferroni correction (4 ROIs).

Decoding fear profiles from image embeddings in deep neural networks. We also aimed to determine if deep neural networks trained to recognize images could be used to predict the fear profiles of participants. We used two different networks with different architectures: a deep convolutional neural network (Visual Geometry Group 19; VGG19) [31] and a transformer-based vision model (Contrastive Language-Image Pretraining; CLIP) [32]. For both networks, we used pre-trained and fixed versions of the models.

We used the "imagenet-vgg-verydeep-19" version of VGG19 from the MatConvNet website (https://www.vlfeat.org/matconvnet/) trained on the ILSVRC-2012 dataset that included 1,000 image categories of various animals and human-made objects. It includes 19 layers: 16 convolutional and 3 fully connected layers: Conv1 (Conv1_1 and Conv1_2; 3211264 units), Conv2 (Conv2_1 and Conv2_2; 1605632 units), Conv3 (Conv3_1 and Conv3_2; 802816 units), Conv4 (Conv4_1,Conv4_2, Conv4_3, and Conv4_4; 401408 units), Conv5 (Conv5_1, Conv5_2, Conv5_3 and Conv5_4; 100352 units), fc6 (4096 units), fc7 (4096 units) and fc8 (1000 units) (For more details on the network, see [31]). The MatConvNet toolbox for Matlab [33] was used in order to extract the image embeddings.

We used the "openai/clip-vit-base-patch32" version of CLIP available on Hugging Face (https://huggingface.co/openai/clip-vit-base-patch32). Briefly, CLIP is designed to learn visual concepts and their associated textual descriptions by training on a large corpus of images and corresponding textual descriptions from data found on the internet. The model is trained in a contrastive manner that leverages both image and text embeddings to establish meaningful associations between images and their corresponding textual descriptions. It is based on the Vision Transformer (ViT) architecture, a popular model for image classification tasks. The "clip-vit-base-patch32" variant utilizes a patch size of 32x32 pixels for processing images. Here,

we extracted the latent-space embedding of each image, after projection to the latent space with identical dimensions as the text model (512 dimensions).

The embeddings of our 2700 images in the two networks (i.e., in each layer of VGG19 and in the latent space of CLIP) were used to train machine learning decoders to predict the fear profile (i.e., fear ratings of a given participant to each of the 30 animal categories) of the 30 participants in the "Fear" group. For the image embeddings of CLIP, a LASSO regression was implemented in a 6-fold cross-validation framework (as a function of experimental runs) and performances were determined using the Fisher-transformed correlation coefficient between the predicted and real fear rating values. A similar approach was used to determine the prediction capacity of each layer within VGG19. However, since some layers included a great number of units (e.g., 3211264 for Conv1_1 and Conv1_2), we elected to use partial-least square regression as implemented in Scikit-Learn [29] in order to first decrease the dimensionality of the data. Performances were also determined using the Fisher-transformed correlation coefficient.

Image synthesis based on the embedding decoders. In pyTorch, we carried out a procedure to generate latent-space embeddings corresponding to high outputs of specific fear profile decoders. The optimization process included 300 iterations in order to update an initial zero vector in latent space as a function of the loss function computed between a high fear value and the predicted value by the latent-space decoder. As a result, the zero vector was iteratively updated using the backpropagation of this error. The resultant latent-space embeddings were then reconstructed visually using the Stable UnCLIP pipeline available on Hugging face (https://huggingface.co/docs/diffusers/api/pipelines/stable_unclip). This approach allows to leverage Stable Diffusion 2 (https://huggingface.co/docs/diffusers/api/pipelines/stable_diffusion/stable_diffusion_2) in order to generate visual images conditioned on the CLIP vision

embeddings [34]. This procedure was used in order to synthesize the visual features leading to high outputs of the latent-space fear profile decoders.

Information transmission to other brain regions. We used information transmission analysis [8,10,35,36] to determine between-group differences in the communication of the ventral visual regions with other brain regions. Essentially, this analysis uses a machine learning approach (i.e., LASSO regression) to predict decoded information in a seed region (i.e., predicted fear ratings in the fusiform region) from another brain region. As a result, this analysis can indicate the communication of information between two brain regions if the activity in one region can indeed predict the decoded information in another. This was achieved in a 6-fold cross-validation using functions from Scikit-Learn [29] and performances were assessed using Fisher-transformed correlation coefficients.

We compared the mean transmission results in the "No Fear" group to the corresponding participants in the "Fear" group using paired-sample t-tests. Significance was determined after correcting for multiple comparisons using the Bonferroni approach (9 ROIs and 4 seed regions).

Results

Decoding fear profiles in the ventral visual stream. The brain decoders could predict fear profiles above chance in the 4 regions in the ventral visual stream, namely the occipital cortex ($t(29) = 14.293$, $p = 4.64 \times 10e\text{-}14$; Bonferroni corrected, Mean = 0.285, STD =0.11, Cohen's d = 2.61), the fusiform gyrus ($t(29) = 10.425$, $p = 1.019 \times 10e\text{-}10$, Bonferroni corrected, Mean = 0.211, STD = 0.11, Cohen's d = 1.90), the inferior temporal gyrus ($t(29) = 6.422$, $p = 2.018 \times 10e\text{-}06$, Bonferroni corrected, Mean = 0.10, STD = 0.089, Cohen's d = 1.17) and the middle temporal gyrus ($t(29) = 7.124$, $p = 3.081 \times 10e\text{-}07$, Bonferroni corrected Mean = 0.115, STD = 0.088, Cohen's d = 1.30). Fear profiles were not predicted more accurately in participants

reporting subjective fear of the animals compared with participants reporting no fear in any of the 4 regions ("Fear" group vs "No Fear" group; Occipital: $t(29) = 1.93$, $p = 0.252$, Bonferroni corrected; Fusiform: $t(29) = 1.425$, $p = 0.660$, Bonferroni corrected; Inferotemporal: $t(29) = 0.023$, $p = 0.999$, Bonferroni corrected; Middle temporal: $t(29) = 1.95$, $p = 0.105$, Bonferroni corrected). Bayesian paired t-test indicated no evidence to reject the null hypothesis in the Occipital cortex ($BF_{10} = 0.99$), Fusiform gyrus ($BF_{10} = 0.48$) and inferior temporal gyrus ($BF_{10} = 0.20$) and anecdotal evidence in favor of the alternative hypothesis (H1) in the middle temporal gyrus ($BF_{10} = 2.00$) [37–39].

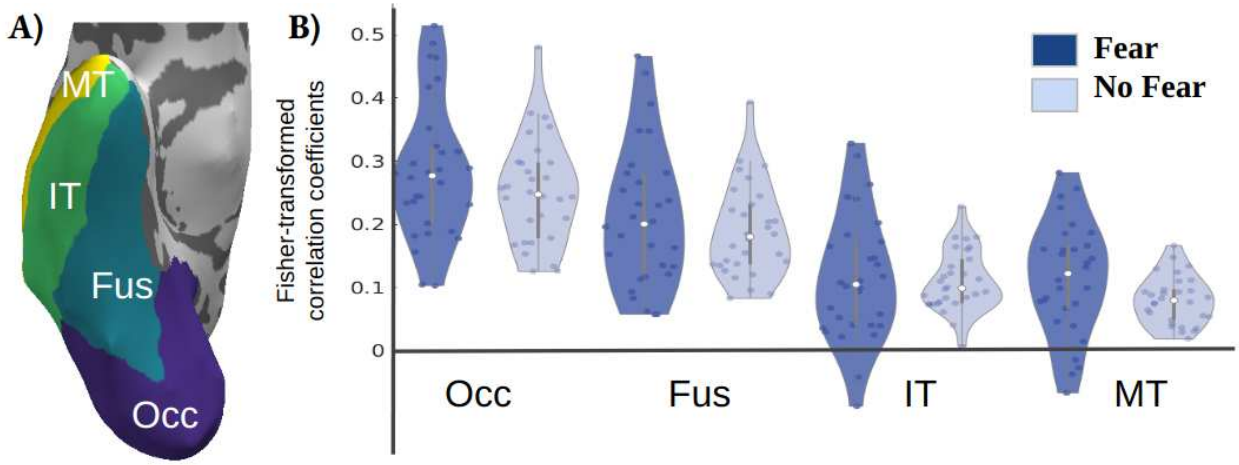

Figure 2. Prediction of the fear profiles in participants with ("Fear group") and without ("No fear" group) subjective fear of the animals. Generally, the fine-grained spatial patterns of hemodynamic activity in all four regions (occipital cortex, Occ; fusiform gyrus, Fus; inferotemporal cortex, IT, and middle temporal cortex, MT) can distinguish, better than chance, between images of threatening and non-threatening animal categories (see main text for statistical information). However, this was true regardless of whether the human participants in questions reported being subjectively afraid of the typically threatening animal categories. This dissociation between subjective fear and stimulus threat was possible because some 'threatening' animals (e.g. cockroaches) were only fearful to some but not all participants. Violin shapes represent density and dots individual participants (Fear group) or group mean (No Fear group). Central dot represents the mean and error bars' edges the 1st and 3rd quantiles. The image of the ROIs was generated based on the Brainnetome atlas using pySurfer (https://github.com/nipy/PySurfer/).

Predicting fear profiles from image embeddings in deep neural networks. The image embeddings in the different layers of VGG19 networks can be used to predict, above chance, the 30 fear profiles of our participants. The t-values ranged between 5.6620 (fc2: t(29) = 5.6620, p = 2.04 x 10e-04; Bonferroni corrected) and 7.203 (conv5_2: t(29) = 7.203 6.10 X 10e-06; Bonferroni corrected) with the Conv5 layers presenting the highest coefficients (Mean = 0.3631 to 0.3846; STD = 0.249 to 0.263). Only FC3 did not present a significant prediction of the fear profiles (t(29) = 1.62; p = 0.120; Bonferroni corrected). Furthermore, the image embeddings in the latent space of the CLIP network could also be used to predict, above chance, the 30 fear profiles of the participants in the "Fear" group (t(29) = 37.404; p = 4.2862 X 10e-26).

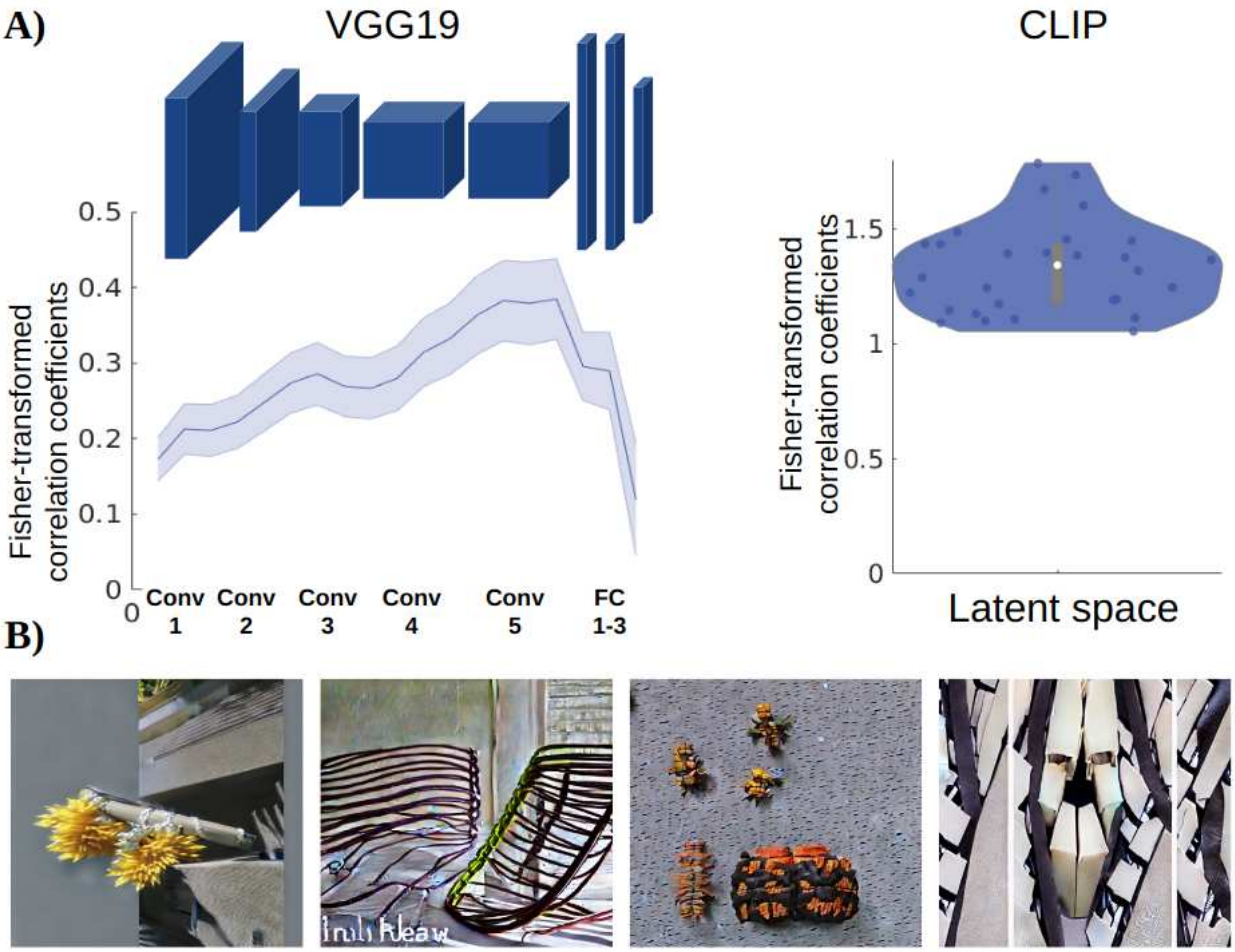

Figure 3. (A) Fear profiles of participants can be predicted from the activity generated by the 2700 images in two artificial ('deep') neural networks: VGG19 and CLIP (the vision 'transformer'). By fear profile we mean the different self-reported subjective fear scores over all the animal categories, for an individual participant. Based on the pattern of activity in 'nodes' within an artificial neural network over many stimuli, we tried to predict these fear profiles for each participant. The Fisher-transformed correlation coefficient is a measure of how well activity from each layer of a network, or activity from the 'latent-space' of a network (see main text for more details), can accurately predict the fear profile over different animal categories. These results indicate that both networks can perform far better than chance (see main text for statistics). (B) Synthetic images generated using the decoders of fear profiles of 4 participants (based on the CLIP embeddings). To understand the nature of the relevant representations within these networks that allowed the above results, we used an optimization procedure and StableUnCLIP to generate synthetic images that represent the 'prototypical' content for some fear profiles of participants. As one can see, these synthetic images do not necessarily resemble animals but include visual features of some of the most feared animals in the participants' profile (from left to right, bee, worm, caterpillar and spider). Based on our own subjective inspection, the synthetic images do not necessarily appear to be fear-inducing.

Information transmission to other brain regions. Information transmission analyses were conducted using the 4 ventral visual stream ROIs as seed regions. Participants in the "Fear" group showed a greater information transmission between the fusiform gyrus and multiple regions in the prefrontal cortex, namely the orbitofrontal ($t(29) = 4.805$, $p = 0.0016$; Bonferroni corrected), the ventromedial ($t(29) = 4.366$, $p = 0.0053$; Bonferroni corrected) and dorsolateral prefrontal cortex ($t(29) = 3.804$, $p = 0.025$; Bonferroni corrected). Furthermore, participants in the "Fear" group also showed a greater information transmission between the fusiform gyrus and the hippocampus ($t(29) = 3.88$, $p = 0.020$; Bonferroni corrected) and between the inferior temporal gyrus and the orbitofrontal cortex ($t(29) = 3.83$, $p = 0.022$; Bonferroni corrected).

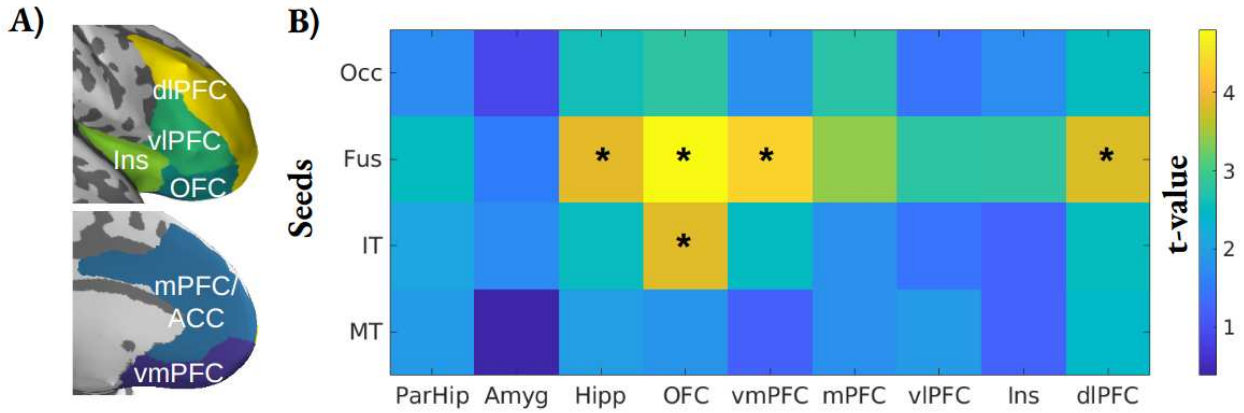

Figure 4. Difference in information transmission from ventral visual regions to other brain areas, between participants with and without subjective fear of 'threatening' stimuli. Color coded represent the t-value of the between group difference in a measure of information transmission. The measure essentially captures how the multivoxel pattern in a seed region (Occ, Fus, IT, MT; same label as used in Figure 2), with respect to the degree to which it can distinguish between threatening vs non-threatening stimuli, can be predicted by the multivoxel pattern in another "target" region (para-hippocampal area, ParHip; amygdala, Amyg; hippocampus, Hipp; orbitofrontal cortex, OFC; ventromedial prefrontal cortex, vmPFC; medial prefrontal cortex, mPFC; ventrolateral prefrontal cortex, vlPFC; insula, Ins; dorsolateral prefrontal cortex, dlPFC). Specifically, what is plotted is not the absolute value of information transmission, but rather the difference in these values between participants who reported to be afraid of the relevant threatening stimuli, and participants who reported not to feel so. Marked in asterisks (*) are pathways that are significantly different between the two groups of participants, after Bonferroni correction (see main text for statistical details). In other words, these information transmission pathways distinguished between different levels of self-reported subjective fear (across participants), while the physical stimuli (including both images of typically threatening and non-threatening animal categories) were held constant. The image of the ROIs was generated based on the Brainnetome atlas using pySurfer (https://github.com/nipy/PySurfer/).

Discussion

In summary, as in some previous studies [1,2], here we found that "fear profiles" can be predicted from patterns of hemodynamic activity generated by threatening and non-threatening stimuli in the human visual and visual association cortices. However, this was the case regardless of whether the human subjects reported to be subjectively afraid of the visual stimuli in question. Further, we found that these stimuli could also be distinguished from the activity patterns within artificial neural networks that were not trained to identify threat or fear *per se* (but rather, just to

identify different objects). Based on the information captured by the decoders of the artificial neural network CLIP, we generated synthetic stimuli to illustrate the visual information distinguishing threatening and non-threatening stimuli. Interestingly, these generated stimuli also do not seem to look subjectively threatening. Together this seems to support the hypothesis that the early visual representations do not actually encode fear, but rather, just visual features that are statistically common in stimuli that can be interpreted as threatening by some individuals.

In contrast, the main positive finding is that subjective fear was reflected by information transmission between different prefrontal regions and ventral visual areas, specifically the fusiform gyrus, and to a lesser extent, the inferotemporal area (IT). This is to say, participants who reported to be subjectively afraid of the relevant animals showed heightened information transmissions in these pathways as they watched the threatening stimuli. This finding may add some credence to the view that subjective experiences require implicit metacognitive processes that depend on the prefrontal cortex [5–7,40].

Notably, we did not observe this difference in information transmission from ventral visual areas to the amygdala and insula. These areas have traditionally been thought to be important for fear processing [41,42]. However, much of the evidence behind that idea came from studies of animal models, most notably in rodents [43–46]. In such studies, fear is only indirectly inferred based on physiology or behavior. In a recent study in humans, we have also found that physiological arousal (i.e., skin conductance response) in reaction to viewing threatening stimuli can in fact be predicted by patterns of hemodynamic activity in the amygdala and insula [1]. However, self-reports of subjective fear were better predicted by patterns of hemodynamic activity in prefrontal areas [1].

We also did not observe significant difference in information transmission between

ventral visual areas and the ventrolateral prefrontal cortex. This prefrontal region receives input from the ventral visual areas, especially IT. In a recent study, it was found that chemical inactivation of this prefrontal region in monkeys can impair object recognition, as it dampens feedback responses to IT [47]. However, this mechanism seems to concern objective identification in general, especially in ambiguous images, but not directly affective processing.

Together, these findings could perhaps be considered under Tulving's distinction between anoetic, noetic, and autonoetic conscious processing [48–50]. The information flow from ventral visual areas to amygdala may be considered anoetic (lacking knowledge), as it likely reflects physiological responses that aren't specific, with respect to visual content. The information flow to the ventrolateral prefrontal cortex may be considered noetic (knowing), but it concerns the information about the visual objects rather than oneself. It is the interaction between the ventral visual stream and other prefrontal areas, including ventromedial prefrontal, orbitofrontal, and dorsolateral prefrontal cortices, that reflects autonoetic processes, i.e. processes about oneself [51]. It has been argued that fear as a conscious experience always requires self-related mechanisms [6,51].

The current study has several important limitations. For example, the threatening visual stimuli are all animals. In real life, there are of course other kinds of threatening stimuli, such as weapons. It is possible that images of animals are processed by evolutionarily hardwired mechanisms, and therefore differently from other inanimate stimuli. It remains to be tested in future studies whether the current findings would generalize.

Also, our key positive findings depend on the analysis of information transmission. This analytic method is not totally new, and has been employed in numerous previous studies [8,10,35,36]. It focuses on how information as captured by patterns of hemodynamic activity

(rather than overall level) is reflected by patterns of activity in another region. In this sense, it is a slightly more advanced multivoxel variant of standard connectivity analysis. However, like standard connectivity analysis, it is an correlational method. For understanding causal interactions between brain areas, invasive interventional methods are more powerful and rigorous. Unfortunately, they are not easily employed in human studies. Future studies on animal models can address this issue better.

Finally, in assessing the subject fear level in response to the synthetic images generated by the artificial neural network models (Fig. 3), we did not conduct formal behavioral tests. We only visually inspected the images ourselves, and feel that such formal tests are not necessary, because the images barely resemble the actually threatening images. Also, this is not a main finding for the current study. However, we cannot preclude the existence of subtle arousal effects. We plan to address this limitation in a future study. If these synthetic stimuli are proven not to elicit an excessive level of fear or discomfort, even in patients with phobia of the relevant animals, one interesting possibility may be to test if these synthetic stimuli can be used for the purpose of exposure therapy - without the patients having to directly encounter the unpleasantness of seeing the actual images of the phobic objects.

Acknowledgements and funding statement

V.T-D. was supported in part by the Canadian Institute of Health Research and the *Fond de recherche du Québec - Santé*. A.C. and M.K. are partially supported by the Japan Science and Technology agency ERATO Ikegaya brain-AI fusion (grant number JPJMER1801), by JSPS KAKENHI (grant number JP22H05156), and by the Agency for Technology, Labour and Innovation (grant number JP004596).

Data and code availability

Data and codes to recreate the statistical analyses can be found here:

https://osf.io/5xtgc/?view_only=b7f4fbc85ddc4fbf8fc7074412b1e3ff

References

1. Taschereau-Dumouchel V, Kawato M, Lau H. 2020 Multivoxel pattern analysis reveals dissociations between subjective fear and its physiological correlates. *Mol. Psychiatry* **25**, 2342–2354.

2. Kragel PA, Reddan MC, LaBar KS, Wager TD. 2019 Emotion schemas are embedded in the human visual system. *Sci Adv* **5**, eaaw4358.

3. Pessoa L, Adolphs R. 2010 Emotion processing and the amygdala: from a 'low road' to 'many roads' of evaluating biological significance. *Nat. Rev. Neurosci.* **11**, 773–782.

4. LeDoux JE. 1996 *The Emotional Brain: The Mysterious Underpinnings of Emotional Life*. Simon and Schuster.

5. LeDoux JE, Pine DS. 2016 Using Neuroscience to Help Understand Fear and Anxiety: A Two-System Framework. *Am. J. Psychiatry* **173**, 1083–1093.

6. LeDoux JE, Brown R. 2017 A higher-order theory of emotional consciousness. *Proc. Natl. Acad. Sci. U. S. A.* **114**, E2016–E2025.

7. LeDoux JE. 2015 *Anxious: Using the Brain to Understand and Treat Fear and Anxiety*. Penguin.

8. Shibata K, Watanabe T, Sasaki Y, Kawato M. 2011 Perceptual learning incepted by decoded fMRI neurofeedback without stimulus presentation. *Science* **334**, 1413–1415.

9. Peirce JW. 2007 PsychoPy—Psychophysics software in Python. *J. Neurosci. Methods* **162**, 8–13.

10. Taschereau-Dumouchel V, Cortese A, Chiba T, Knotts JD, Kawato M, Lau H. 2018 Towards an unconscious neural reinforcement intervention for common fears. *Proc. Natl. Acad. Sci. U. S. A.* **115**, 3470–3475.

11. Esteban O *et al.* 2019 fMRIPrep: a robust preprocessing pipeline for functional MRI. *Nat. Methods* **16**, 111–116.

12. Gorgolewski K, Burns CD, Madison C, Clark D, Halchenko YO, Waskom ML, Ghosh SS. 2011 Nipype: a flexible, lightweight and extensible neuroimaging data processing framework in python. *Front. Neuroinform.* **5**, 13.

13. Gorgolewski KJ *et al.* 2018 Nipype. *Softw. Pract. Exp.*

14. Tustison NJ, Avants BB, Cook PA, Zheng Y, Egan A, Yushkevich PA, Gee JC. 2010 N4ITK: improved N3 bias correction. *IEEE Trans. Med. Imaging* **29**, 1310–1320.

15. Avants BB, Epstein CL, Grossman M, Gee JC. 2008 Symmetric diffeomorphic image registration with cross-correlation: evaluating automated labeling of elderly and neurodegenerative brain. *Med. Image Anal.* **12**, 26–41.

16. Zhang Y, Brady M, Smith S. 2001 Segmentation of brain MR images through a hidden Markov random field model and the expectation-maximization algorithm. *IEEE Trans. Med. Imaging* **20**, 45–57.

17. Dale AM, Fischl B, Sereno MI. 1999 Cortical surface-based analysis. I. Segmentation and surface reconstruction. *Neuroimage* **9**, 179–194.

18. Klein A *et al.* 2017 Mindboggling morphometry of human brains. *PLoS Comput. Biol.* **13**, e1005350.

19. Fonov VS, Evans AC, McKinstry RC, Almli CR, Collins DL. 2009 Unbiased nonlinear average age-appropriate brain templates from birth to adulthood. *Neuroimage* **Supplement 1**, S102.

20. Greve DN, Fischl B. 2009 Accurate and robust brain image alignment using boundary-based registration. *Neuroimage* **48**, 63–72.

21. Jenkinson M, Bannister P, Brady M, Smith S. 2002 Improved optimization for the robust and accurate linear registration and motion correction of brain images. *Neuroimage* **17**, 825–841.

22. Cox RW, Hyde JS. 1997 Software tools for analysis and visualization of fMRI data. *NMR Biomed.* **10**, 171–178.

23. Lanczos C. 1964 Evaluation of Noisy Data. *Journal of the Society for Industrial and Applied Mathematics Series B Numerical Analysis* **1**, 76–85.

24. Abraham A, Pedregosa F, Eickenberg M, Gervais P, Mueller A, Kossaifi J, Gramfort A, Thirion B, Varoquaux G. 2014 Machine learning for neuroimaging with scikit-learn. *Front. Neuroinform.* **8**, 14.

25. Mumford JA, Turner BO, Ashby FG, Poldrack RA. 2012 Deconvolving BOLD activation in event-related designs for multivoxel pattern classification analyses. *Neuroimage* **59**, 2636–2643.

26. Turner BO, Mumford JA, Poldrack RA, Ashby FG. 2012 Spatiotemporal activity estimation for multivoxel pattern analysis with rapid event-related designs. *Neuroimage* **62**, 1429–1438.

27. Hanke M, Halchenko YO, Sederberg PB, Hanson SJ, Haxby JV, Pollmann S. 2009 PyMVPA: A python toolbox for multivariate pattern analysis of fMRI data. *Neuroinformatics* **7**, 37–53.

28. Hanke M *et al.* 2009 PyMVPA: A Unifying Approach to the Analysis of Neuroscientific Data. *Front. Neuroinform.* **3**, 3.

29. Pedregosa F, Varoquaux G, Gramfort A. 2011 Scikit-learn: Machine learning in Python. *the Journal of machine*

30. Fan L *et al.* 2016 The Human Brainnetome Atlas: A New Brain Atlas Based on Connectional Architecture. *Cereb. Cortex* **26**, 3508–3526.

31. Simonyan K, Zisserman A. 2014 Very Deep Convolutional Networks for Large-Scale Image Recognition. *arXiv [cs.CV]*.

32. Radford A *et al.* 18--24 Jul 2021 Learning Transferable Visual Models From Natural Language Supervision. In *Proceedings of the 38th International Conference on Machine Learning* (eds M Meila, T Zhang), pp. 8748–8763. PMLR.

33. Vedaldi A, Lenc K. 2015 MatConvNet: Convolutional Neural Networks for MATLAB. In *Proceedings of the 23rd ACM international conference on Multimedia*, pp. 689–692. New York, NY, USA: Association for Computing Machinery.

34. Ramesh A, Dhariwal P, Nichol A, Chu C, Chen M. 2022 Hierarchical Text-Conditional Image Generation with CLIP Latents. *arXiv [cs.CV]*.

35. Cortese A, Amano K, Koizumi A, Kawato M, Lau H. 2016 Multivoxel neurofeedback selectively modulates confidence without changing perceptual performance. *Nat. Commun.* **7**, 13669.

36. Koizumi A, Amano K, Cortese A, Shibata K, Yoshida W, Seymour B, Kawato M, Lau H. 2016 Fear reduction without fear through reinforcement of neural activity that bypasses conscious exposure. *Nat Hum Behav* **1**. (doi:10.1038/s41562-016-0006)

37. Lee MD, Wagenmakers E-J. 2014 *Bayesian Cognitive Modeling: A Practical Course*. Cambridge University Press.

38. Jeffreys H. 1998 *The Theory of Probability*. OUP Oxford.

39. Stefan AM, Gronau QF, Schönbrodt FD, Wagenmakers E-J. 2019 A tutorial on Bayes Factor Design Analysis using an informed prior. *Behav. Res. Methods* **51**, 1042–1058.

40. Taschereau-Dumouchel V, Michel M, Lau H, Hofmann SG, LeDoux JE. 2022 Putting the 'mental' back in 'mental disorders': a perspective from research on fear and anxiety. *Mol. Psychiatry* (doi:10.1038/s41380-021-01395-5)

41. Rogan MT, Stäubli UV, LeDoux JE. 1997 Fear conditioning induces associative long-term potentiation in the amygdala. *Nature* **390**, 604–607.

42. Phelps EA, O'Connor KJ, Gatenby JC, Gore JC, Grillon C, Davis M. 2001 Activation of the

left amygdala to a cognitive representation of fear. *Nat. Neurosci.* **4**, 437–441.

43. Panksepp J. 2012 What is an emotional feeling? Lessons about affective origins from cross-species neuroscience. *Motiv. Emot.* **36**, 4–15.

44. Davis M. 1992 The Role of the Amygdala in Fear and Anxiety. *Annu. Rev. Neurosci.* **15**, 353–375.

45. Fanselow MS, Poulos AM. 2005 The neuroscience of mammalian associative learning. *Annu. Rev. Psychol.* **56**, 207–234.

46. Tovote P, Fadok JP, Lüthi A. 2015 Neuronal circuits for fear and anxiety. *Nat. Rev. Neurosci.* **16**, 317–331.

47. Kar K, DiCarlo JJ. 2021 Fast Recurrent Processing via Ventrolateral Prefrontal Cortex Is Needed by the Primate Ventral Stream for Robust Core Visual Object Recognition. *Neuron* **109**, 164–176.e5.

48. Terrace HS, Metcalfe J. 2005 *The Missing Link in Cognition: Origins of Self-Reflective Consciousness*. Oxford University Press.

49. Tulving E. 2004 Origin of autonoesis in episodic memory. In *The nature of remembering: Essays in honor of Robert G. Crowder*, pp. 17–34. Washington: American Psychological Association.

50. Tulving E. 1985 Memory and consciousness. *Canadian Psychology/Psychologie canadienne* **26**, 1.

51. LeDoux JE, Lau H. 2020 Seeing consciousness through the lens of memory. *Curr. Biol.* **30**, R1018–R1022.